

Electrically detected magnetic resonance study on interface defects at nitrated Si-face, α -face, and m -face 4H-SiC/SiO₂ interfaces ^{EP}

Cite as: Appl. Phys. Lett. **116**, 171602 (2020); <https://doi.org/10.1063/5.0002944>

Submitted: 30 January 2020 . Accepted: 08 April 2020 . Published Online: 27 April 2020

E. Higa ^{id}, M. Sometani ^{id}, H. Hirai ^{id}, H. Yano ^{id}, S. Harada ^{id}, and T. Umeda ^{id}

COLLECTIONS

^{EP} This paper was selected as an Editor's Pick



View Online



Export Citation



CrossMark

ARTICLES YOU MAY BE INTERESTED IN

[Prospects for n-type doping of \(Al_xGa_{1-x}\)₂O₃ alloys](#)

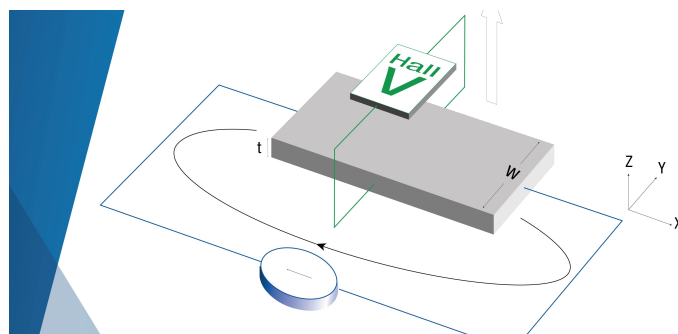
Applied Physics Letters **116**, 172104 (2020); <https://doi.org/10.1063/5.0006224>

[Molecular beam homoepitaxy on bulk AlN enabled by aluminum-assisted surface cleaning](#)

Applied Physics Letters **116**, 172106 (2020); <https://doi.org/10.1063/1.5143968>

[Synergistically promoted thermoelectric performance of SnTe by alloying with NaBiTe₂](#)

Applied Physics Letters **116**, 173902 (2020); <https://doi.org/10.1063/1.5144697>



**Tips for minimizing
Hall measurement errors**

Download the Technical Note

Lake Shore
CRYOTRONICS

Electrically detected magnetic resonance study on interface defects at nitrated Si-face, α -face, and m -face 4H-SiC/SiO₂ interfaces

Cite as: Appl. Phys. Lett. **116**, 171602 (2020); doi: [10.1063/5.0002944](https://doi.org/10.1063/5.0002944)

Submitted: 30 January 2020 · Accepted: 8 April 2020 ·

Published Online: 27 April 2020









View Online



Export Citation



CrossMark

E. Higa,¹  M. Sometani,²  H. Hirai,²  H. Yano,¹  S. Harada,²  and T. Umeda^{1,a)} 

AFFILIATIONS

¹Institute of Applied Physics, University of Tsukuba, Tsukuba 305-8573, Japan

²National Institute of Advanced Industrial Science and Technology (AIST), Tsukuba 305-8569, Japan

^{a)} Author to whom correspondence should be addressed: umeda@bk.tsukuba.ac.jp

ABSTRACT

We investigated interface defects formed on a -face and m -face 4H-SiC/SiO₂ interfaces after interface nitridation by nitric oxide (NO) post-oxidation annealing (POA). Using electrically detected magnetic-resonance spectroscopy, we observed interface defects on these faces. The a - and m -face interface defects were found to be similar to a carbon-related interface defect (the P_{bc} center) observed on the standard Si-face, but their amounts were significantly lower than those of the Si-face after the same NO POA. Such a reduction was correlated with a drastic increase in the field-effect mobility ($80\text{--}90\text{ cm}^2\text{ V}^{-1}\text{ s}^{-1}$) of the a - and m -face metal-oxide-semiconductor field-effect transistors after NO POA. We also found that over-nitridation caused the formation of two types of nitrogen-related defects on the Si-face. These nitrogen-related defects resemble the K center (Si dangling-bond center) observed in Si₃N₄.

Published under license by AIP Publishing. <https://doi.org/10.1063/5.0002944>

Silicon carbide metal-oxide-semiconductor field-effect transistors (4H-SiC MOSFETs) have many advantages such as lower energy loss, higher power, higher frequency, and higher temperature operation for power electronics compared to conventional silicon (Si)-based power electronics.^{1,2} However, their performances are severely limited due to their field-effect mobility (μ_{FE}) being much lower than the ideal electron mobility ($\sim 1000\text{ cm}^2\text{ V}^{-1}\text{ s}^{-1}$).³ Improvement in μ_{FE} can be achieved using two basic techniques: introducing a high density of nitrogen (N) atoms into the interface^{4–7} and using either a 4H-SiC(1120) surface (“ a -face”) or a 4H-SiC(1100) surface (“ m -face”) for the MOSFET channel.^{2,8,9} By using interface nitridation by post-oxidation annealing (POA) with nitric oxide (NO),^{4–7} the maximum μ_{FE} increases from $1\text{--}7\text{ cm}^2\text{ V}^{-1}\text{ s}^{-1}$ for standard 4H-SiC(0001) (the so-called “Si-face”) MOSFETs¹⁰ to $25\text{--}40\text{ cm}^2\text{ V}^{-1}\text{ s}^{-1}$ for nitrated Si-face MOSFETs. Furthermore, the use of the a -face or m -face together with interface nitridation increases the maximum μ_{FE} to $100\text{ cm}^2\text{ V}^{-1}\text{ s}^{-1}$.^{8,9} However, the microscopic mechanism of such an improvement is not fully clear. To reveal microscopic information on interface defects, electrically detected magnetic-resonance (EDMR) spectroscopy has been applied to fully processed 4H-SiC MOSFETs.^{11–16} Previous EDMR studies revealed interface defects such as the “interface Si-vacancy center,”^{11–13} “ P_{bc} center” [interface

carbon dangling-bond (C DB) center],^{14,15} and “dual- P_{bc} center.”¹⁶ However, all of them were found on the Si-face, and no EDMR data have been reported for the a - and m -faces thus far.

In this Letter, we present EDMR observations on the a - and m -face interfaces after NO POA. Both interfaces revealed EDMR signals of C-related interface defects similar to the P_{bc} center observed on the Si-face.^{14,15} However, the amounts of C-related defects were found to be two orders of magnitude lower on the nitrated a - and m -faces than on the Si-face. We, therefore, suggest that the drastic improvement in the maximum μ_{FE} ($79\text{ cm}^2\text{ V}^{-1}\text{ s}^{-1}$ for the a -face and $89\text{ cm}^2\text{ V}^{-1}\text{ s}^{-1}$ for the m -face) is mainly caused by eliminating C-related defects. However, we found that interface nitridation is less effective for the Si-face and over-nitridation even created additional interface defects related to N atoms. We speculate that these additional defects may be similar to the K center (Si DB center in Si₃N₄)^{17,18} and related to the negative effects of over-nitridation.¹⁹

We prepared n -channel lateral 4H-SiC MOSFETs on Si-, a -, and m -face wafers, as shown in Table I. The Si-face MOSFETs were fabricated on 4° -off p^- epitaxial layers (Al concentration = $4\text{--}5 \times 10^{15}\text{ cm}^{-3}$) on 4H-SiC(0001) wafers. The a - and m -face wafers were prepared by cutting 4H-SiC crystal ingots each with an off angle of about 10° . On these substrates, p^- epitaxial layers were grown with Al

TABLE I. 4H-SiC MOSFET samples studied by EDMR.

Label	NO POA time (min)	μ_{FE} ($\text{cm}^2 \text{V}^{-1} \text{s}^{-1}$)
Si-face dry ^{14,15}	0	6.8
Si-face NO10	10	28
Si-face NO60	60	32
Si-face NO120	120	31
<i>a</i> -face NO60	60	79
<i>m</i> -face NO60	60	89

concentrations of $1.3 \times 10^{16} \text{ cm}^{-3}$ for the *a*-face and $1.8 \times 10^{16} \text{ cm}^{-3}$ for the *m*-face. For all the MOSFETs, gate oxides (50 nm) were grown by standard dry oxidation. After dry oxidation, NO POA was carried out at 1250°C for each duration shown in Table I. Before the NO POA, *a*- and *m*-face MOSFETs hardly activated the channel currents. We call the MOSFETs prepared by the NO POA times of 0, 10, 60, and 120 min “dry,” “NO10,” “NO60,” and “NO120,” respectively. The gate electrodes were fabricated by poly-Si deposition. The gate length (*L*) and width (*W*) were $5 \mu\text{m}$ and $2000 \mu\text{m}$, respectively, except for the *m*-face MOSFET (*L* = $5 \mu\text{m}$ and *W* = $200 \mu\text{m}$). A top view of the MOSFET is shown in Fig. 1(a). The maximum μ_{FE} values for each MOSFET were evaluated and are listed in Table I.

EDMR measurements were carried out at room temperature by using an X-band EDMR spectrometer we constructed and used in our previous studies.^{14,15} We adopted bipolar-amplification-effect (BAE)

EDMR measurements that were optimized to detect interface signals with a high signal-to-noise ratio (*S/N*).^{20,21} In this regime, we activated a constant current (*I_d*) from the drain to the well and monitored electron-spin-resonance (ESR)-induced current changes in the drain-source current (*I_{EDMR}*), as shown in Fig. 1(a). The gate voltage (*V_g*) was optimized to maximize the *S/N*. We used lock-in detection synchronized with magnetic-field modulation at 1.56 kHz. ESR transitions were excited by microwave at 9.462 GHz and 200 mW.

Figure 1(b) shows the EDMR spectra for the Si-, *a*-, and *m*-face “NO60” MOSFETs together with the “Si-face dry” MOSFET^{14,15} when the external magnetic field (**B**) was parallel to the [0001] axis (*c* axis). It is immediately clear that the NO POA significantly reduced an EDMR signal of the *P_{bc}* center, which was dominantly observed on the Si-face dry sample.^{14,15} As plotted in Fig. 1(c), the signal intensity on the Si-face decreased to 1/40 (2.5%) after NO POA for 60 min. A consistent result was previously obtained using conventional ESR spectroscopy where an interface signal with a spin density of $3\text{--}4 \times 10^{12} \text{ cm}^{-2}$ was reduced below the detection limit ($<2 \times 10^{11} \text{ cm}^{-2}$) after optimum NO POA or POCl_3 POA.²² In the present study, thanks to the higher *S/N* of EDMR spectroscopy,^{20,21} we could still observe the defect signal even after optimum NO POA. We could also confirm that the *a*- and *m*-faces after the NO60 process displayed a reduced interface EDMR signal, compared to the untreated Si-face,^{14,15} to 1/110 (0.91%) and 1/380 (0.26%), respectively [see Fig. 1(c)]. These EDMR observations suggest that NO POA can remove the *P_{bc}* center and its formation can be much more suppressed on the nitrated *a*- and *m*-faces than on the nitrated Si-face. This provides microscopic information on why the nitrated *a*- and *m*-faces show excellent μ_{FE} . In fact, as shown in Fig. 1(c), maximum μ_{FE} values are correlated with the EDMR signal intensities.

To examine the origins of the interface defects observed on the *a*- and *m*-faces, normalized EDMR spectra measured for **B** parallel to or perpendicular to the *c* axis are shown in Fig. 2. Similar to the *P_{bc}* center observed on Si-face dry, which shows slightly anisotropic *g* factors of $g_{\parallel} = 2.0029$ and $g_{\perp} = 2.0032$,^{14,15} the *a*- and *m*-face NO60 interfaces exhibited similar EDMR signals in the same range of *g* factors (2.0025–2.0031). These *g* factors were close to the free-electron *g* factor (2.0023), and their anisotropy was found to be very weak. These features are characteristic of C-related ESR centers.²² Therefore, we conclude that C-related defects similar to the *P_{bc}* center are formed on the nitrated *a*- and *m*-faces although their structural details could not be resolved due to too small signal intensities. On the Si-face, the microscopic origin of the *P_{bc}* center has been identified as a C DB on a C-adatom structure.¹⁵ We deduced that the surface structures of the *a*- and *m*-faces prevent the formation of C adatoms.

We further investigated the effect of N incorporation using the Si-face. The Si-face NO60 interface (Fig. 2) revealed additional shoulders on both sides of the central signal. These shoulders are asymmetric and should differ from a pair of symmetric shoulders of the *P_{bc}* center, which arise from its hyperfine (HF) interaction.¹⁴ Thus, we judged that the Si-face NO60 interface involves a different signal(s). Figure 3(a) shows the EDMR spectra of the nitrated Si-face MOSFETs with different POA times. EDMR signal intensities increased with the increasing POA time. The NO10 spectrum was identical to the *P_{bc}* spectrum with a reduced intensity (1.2% of the *P_{bc}* intensity in the Si-face dry sample^{14,15}). In this sample, the maximum μ_{FE} suddenly increased to $28 \text{ cm}^2 \text{V}^{-1} \text{s}^{-1}$ (see Table I), supporting our idea that C-related defects strongly affect μ_{FE} .

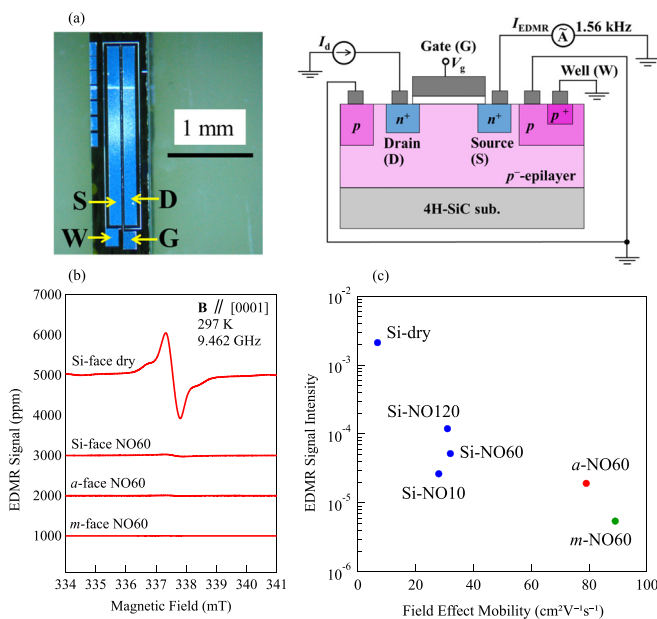


FIG. 1. (a) Photograph of a 4H-SiC MOSFET examined here and its schematic cross section. We adopted the BAE EDMR setup shown here. (b) EDMR spectra of Si-face, *a*-face, and *m*-face MOSFETs. The traces are vertically offset for clarity. Each spectrum was measured under optimized bias conditions such that $V_g = -7.5 \text{ V}$ and $I_{EDMR} = 200 \text{ nA}$ for Si-face dry,^{14,15} $V_g = -5 \text{ V}$ and $I_{EDMR} = 500 \text{ nA}$ for Si-face NO60, $V_g = -5 \text{ V}$ and $I_{EDMR} = 50 \text{ nA}$ for *a*-face NO60, and $V_g = -5.5 \text{ V}$ and $I_{EDMR} = 6 \mu\text{A}$ for *m*-face NO60. (c) Correlation between EDMR signal intensities and maximum field-effect mobilities. These intensities express the peak-to-peak intensities of EDMR signals.

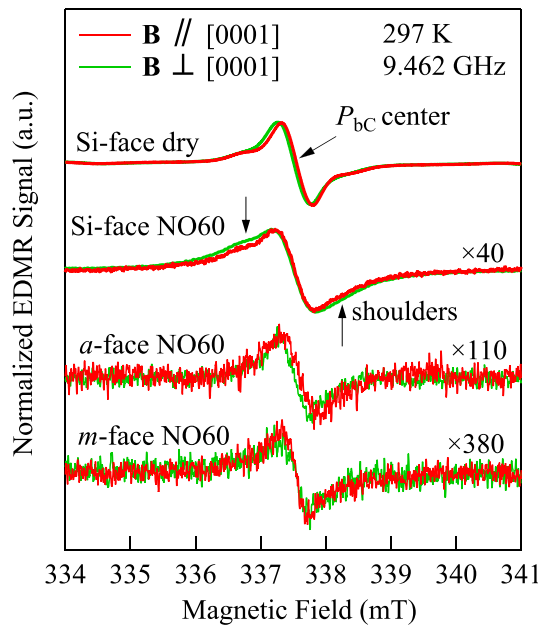


FIG. 2. Normalized EDMR spectra of Si-face, a-face, and m-face MOS interfaces when $\mathbf{B} \parallel [0001]$ or $\mathbf{B} \perp [0001]$. The traces are vertically offset for clarity. Bias conditions were the same as those in Fig. 1(b). The modulation amplitude was set to 0.5 mT except for the m-face (0.25 mT).

We found, however, that the NO60 and NO120 spectra cannot be fitted by the P_{bc} spectrum; alternatively, they could be well fitted by a combination of one broad central signal (dotted line) and another triplet signal (three colored lines). The latter signal is necessary for reproducing the asymmetric shoulders. In addition to the spectra

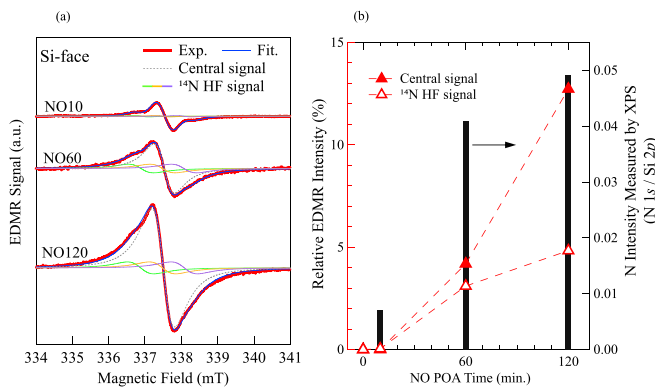


FIG. 3. EDMR study on N-related interface defects on the nitrated Si-face. (a) EDMR spectra for $\mathbf{B} \parallel [0001]$ and fitting results. The traces are vertically offset for clarity. NO10 spectrum could be simply fitted by the P_{bc} signal (observed in the Si-face dry sample^{14,15}). For NO60 and NO120, fitted spectra were calculated by the sum of the “central signal” and the “ ^{14}N HF signal.” EDMR spectra were measured by $V_g = -5$ V and $I_{EDMR} = 10$ μA for NO10, $V_g = -5$ V and $I_{EDMR} = 500$ nA for NO60, and $V_g = -5.5$ V and $I_{EDMR} = 500$ nA for NO120. The modulation amplitude was set to 0.5 mT. (b) Relative EDMR intensities of the central signal and triplet ^{14}N HF signal vs NO POA time. These intensities were normalized by integrated EDMR intensity of the P_{bc} signal in the Si-face dry sample shown in Fig. 1(b).

shown in Fig. 3(a), other EDMR spectra for different magnetic-field angles (30° , 60° , and 90° , where 0° and 90° correspond to $\mathbf{B} \parallel [0001]$ and $\mathbf{B} \parallel [11\bar{2}0]$, respectively) could also be reasonably fitted by the sum of the two signals. The former central signal shows an isotropic g factor of 2.003 and a signal width broader than the P_{bc} signal. The latter triplet signal represents a ^{14}N HF splitting due to a ^{14}N nuclear spin (spin number $I = 1$; natural abundance = 99.6%). Its g factor and ^{14}N HF splitting were found to be isotropic at $g = 2.0032$ and 0.57 mT, respectively.

As shown in Fig. 3(b), these two signals increased with the increasing POA time or the amount of interfacial N atoms shown on the right-side axis. The amount was measured by x-ray photoelectron spectroscopy (XPS) on the same series of nitrated samples.²³ Accordingly, we argue that the central and ^{14}N HF signals are related to incorporated N atoms. The g factor of 2.003 coincides with that of the K center in Si_3N_4 (Si DB center, $\text{N}_3\equiv\text{Si}\cdot$, where “ \cdot ” represents an unpaired electron).^{17,18} Thus, it is reasonable to consider that the central signal may arise from the K center formed inside N-incorporated regions, as schematically drawn in Fig. 4.

We also argue that the ^{14}N HF signal also corresponds to a family of K centers because its ^{14}N HF splitting of 0.57 mT is similar to ^{14}N HF splitting due to back-bonded N atoms of the K center (0.46 mT).¹⁷ Since the ^{14}N HF signal revealed a single ^{14}N HF splitting, we imagine that its origin may be ascribed as an incomplete type of K center, such as $\text{C}_2\text{N}_1\equiv\text{Si}\cdot$. This type of defect may be formed at the boundary between N-incorporated and non-incorporated regions, as shown on the right-hand side of Fig. 4. Since this incomplete K center has only a single back-bonded N atom, we could resolve its ^{14}N HF splitting. If we consider other types of N-related defects such that their unpaired electron mainly distributes on a N atom, much larger ^{14}N HF splitting should be observed. For instance, larger isotropic ^{14}N HF splitting was detected, e.g., 3 mT for a bridging N center ($\text{Si}_2=\text{N}\cdot$ in Si_3N_4),²⁵ 3.3 mT for a substitutional N atom surrounded by C atoms ($\text{C}_4\text{N}\cdot$ in

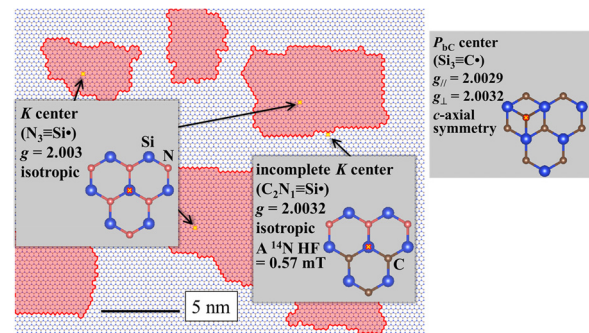


FIG. 4. Schematic image of the nitrated Si-face (NO120) and formation of two types of N-related defects, in addition to the P_{bc} center (rightmost edge).¹⁵ On this surface, the N-atom density was set to $4 \times 10^{14} \text{ cm}^{-2}$ (approximately 35% of surface C atoms were replaced with N atoms).²⁴ N-incorporated honeycomb units are represented as red regions. EDMR detected two types of N-related defects. We argue that one type is similar to the K center ($\text{N}_3\equiv\text{Si}\cdot$) formed inside red regions, and another type is formed at the boundary between red and non-red regions. We also argue that the latter is an incomplete K center (e.g., $\text{C}_2\text{N}_1\equiv\text{Si}\cdot$). Symbols “ \cdot ” represent the unpaired electrons. Fractions of former and latter defects were 3 defects/7128 Si atoms ($0.44 \times 10^{12} \text{ cm}^{-2}$) and 1 defect/7128 Si atoms ($0.17 \times 10^{12} \text{ cm}^{-2}$), respectively. ESR signatures of three EDMR centers are also summarized. See the details in the text.

diamond),²⁶ and 1.8 mT for a substitutional N atom surrounded by Si atoms ($\text{Si}_4\text{N}\bullet$ in 4H-SiC).²⁷ Therefore, we consider the model shown in Fig. 4 to be plausible.

It is known that the K center is an amphoteric charge trap with negative- U behavior.¹⁸ Thus, this type of defects may also reduce the free-electron density in the inversion channel layer by capturing electrons, similar to the case of the P_{bC} center.^{14,15} The valence-band-side energy levels of P_{bC} largely decrease the free-electron density ($7 \times 10^{12} \text{ cm}^{-2}$ for $V_{\text{g}} = 15 \text{ V}$),⁷ resulting in the drastic reduction in μ_{FE} .^{14,15} In contrast, the K -center-related defects appeared to have a weaker impact on μ_{FE} , as shown in Fig. 1(c). It is probably because the density of the K -center-related defects shown in Fig. 4 is one order of magnitude smaller than that of the P_{bC} center. Judging from relative EDMR intensities of the central and ^{14}N HF signals, we roughly estimated the spin densities of the K center and the incomplete K center to be $0.4 \times 10^{12} \text{ cm}^{-2}$ and $0.2 \times 10^{12} \text{ cm}^{-2}$, respectively, for the NO120 interface, supposing that the P_{bC} EDMR intensity in the Si-face dry sample corresponds to $3.5 \times 10^{12} \text{ cm}^{-2}$.^{14,15,22}

At least, the K -center-related defects may be related to the threshold-voltage (V_{th}) instability observed for the over-nitridation of the Si-face¹⁹ because V_{th} is highly sensitive to the presence of the charge traps. For the NO120 interface, the total estimated density ($0.6 \times 10^{12} \text{ cm}^{-2}$) of the K -center-related defects corresponds to a V_{th} shift of 1.4 V for the oxide capacitance of $6.9 \times 10^{-8} \text{ F}\cdot\text{cm}^{-2}$ (the oxide thickness of 50 nm), which may be practically detectable.

In summary, we investigated interface defects formed in nitrided Si-face, a -face, and m -face 4H-SiC MOSFETs using EDMR. For the nitrided a - and m -faces, the EDMR signal of the P_{bC} -related center drastically decreased compared to the Si-face dry interface, resulting in a significant improvement in μ_{FE} from 7 to 80–90 $\text{cm}^2 \text{ V}^{-1} \text{ s}^{-1}$. For the nitrided Si-face, the P_{bC} signal rapidly decreased to 1/80 after 10 min NO POA. By increasing the NO POA time up to 60–120 min, the formation of two types of N-related interface defects was detected by EDMR. We argued that both N-related defects may be similar to the K center ($\text{N}_3\equiv\text{Si}\bullet$) observed in Si_3N_4 . These K -center-related defects may cause reliability issues of Si-face 4H-SiC MOSFETs after over-nitridation.

We would like to thank C. Shinei for useful discussions. This work was supported by the Council for Science, Technology and Innovation (CSTI), Cross-ministerial Strategic Innovation Promotion Program (SIP), and “Next-generation power electronics” (funding agency: NEDO). This work was also partly supported by Grants-in-Aid (Grant Nos. 17H02781 and 20H00340) from the Ministry of Education, Culture, Sports, Science and Technology of Japan.

REFERENCES

- 1T. Kimoto, *Jpn. J. Appl. Phys., Part 1* **54**, 040103 (2015).
- 2H. Yano, T. Hirao, T. Kimoto, H. Matsunami, K. Asano, and Y. Sugawara, *IEEE Electron Device Lett.* **20**, 611 (1999).
- 3T. Hatakeyama, T. Watanabe, M. Kushibe, K. Kojima, S. Imai, T. Suzuki, T. Shinohe, T. Tanaka, and K. Arai, *Mater. Sci. Forum* **433–436**, 443 (2003).
- 4G. Y. Chung, C. C. Tin, J. R. Williams, K. McDonald, R. K. Chanana, R. A. Weller, S. T. Pantelides, L. C. Feldman, O. W. Holland, M. K. Das, and J. W. Palmour, *IEEE Electron Device Lett.* **22**, 176 (2001).
- 5D. Okamoto, H. Yano, T. Hatayama, and T. Fuyuki, *Appl. Phys. Lett.* **96**, 203508 (2010).
- 6R. Kosugi, T. Umeda, and Y. Sakuma, *Appl. Phys. Lett.* **99**, 182111 (2011).
- 7T. Hatakeyama, Y. Kiuchi, M. Sometani, S. Harada, D. Okamoto, H. Yano, Y. Yonezawa, and H. Okumura, *Appl. Phys. Express* **10**, 046601 (2017).
- 8Y. Nanen, M. Kato, J. Suda, and T. Kimoto, *IEEE Trans. Electron Devices* **60**, 1260 (2013).
- 9S. Nakazawa, T. Okuda, J. Suda, T. Nakamura, and T. Kimoto, *IEEE Trans. Electron Devices* **62**, 309 (2015).
- 10S. Harada, R. Kosugi, J. Senzaki, W. Cho, K. Fukuda, K. Arai, and S. Suzuki, *J. Appl. Phys.* **91**, 1568 (2002).
- 11C. J. Cochrane, P. M. Lenahan, and A. J. Lelis, *J. Appl. Phys.* **109**, 014506 (2011).
- 12C. J. Cochrane, P. M. Lenahan, and A. J. Lelis, *Appl. Phys. Lett.* **100**, 023509 (2012).
- 13M. A. Anders, P. M. Lenahan, and A. J. Lelis, *Appl. Phys. Lett.* **109**, 142106 (2016).
- 14T. Umeda, Y. Nakano, E. Higa, T. Okuda, T. Kimoto, T. Hosoi, H. Watanabe, M. Sometani, and S. Harada, *J. Appl. Phys.* **127**, 145301 (2020).
- 15T. Umeda, T. Kobayashi, M. Sometani, H. Yano, Y. Matsushita, and S. Harada, *Appl. Phys. Lett.* **116**, 071604 (2020).
- 16J. Cottom, G. Gruber, G. Pobegen, T. Aichinger, and A. L. Shluger, *J. Appl. Phys.* **124**, 045302 (2018).
- 17W. L. Warren and P. M. Lenahan, *Phys. Rev. B* **42**, 1773 (1990).
- 18W. L. Warren, J. Kanicki, J. Robertson, E. H. Poindexter, and P. J. McWhorter, *J. Appl. Phys.* **74**, 4034 (1993).
- 19J. Rozen, S. Dhar, M. E. Zvanut, J. R. Williams, and L. C. Feldman, *J. Appl. Phys.* **105**, 124506 (2009).
- 20T. Aichinger and P. M. Lenahan, *Appl. Phys. Lett.* **101**, 083504 (2012).
- 21M. A. Anders, P. M. Lenahan, C. J. Cochrane, and A. J. Lelis, *IEEE Trans. Electron Devices* **62**, 301 (2015).
- 22T. Umeda, G.-W. Kim, T. Okuda, M. Sometani, T. Kimoto, and S. Harada, *Appl. Phys. Lett.* **113**, 061605 (2018).
- 23K. Moges, M. Sometani, T. Hosoi, T. Shimura, S. Harada, and H. Watanabe, *Appl. Phys. Express* **11**, 101303 (2018).
- 24K. Hamada, A. Mikami, H. Naruoka, and K. Yamabe, *e-J. Surf. Sci. Nanotechnol.* **15**, 109 (2017).
- 25W. L. Warren, P. M. Lenahan, and S. E. Curry, *Phys. Rev. Lett.* **65**, 207 (1990).
- 26W. V. Smith, P. P. Sorokin, I. L. Gelles, and G. J. Lasher, *Phys. Rev.* **115**, 1546 (1959).
- 27S. Greulich-Weber, *Phys. Status Solidi A* **162**, 95 (1997).